Measurement of Thermal (Brownian) Motion and Diffusion Coefficient of Microspheres

Isabella Schick & Oakley Gompels
University of Toronto
PHY324

2025-11-03

Abstract

We analyzed the Brownian motion of microspheres suspended in liquid using digital video microscope. The mean squared displacement (MSD) of ten particles (T1–T10) was determined from automated position tracking data. Weighted linear fits to $r^2(t) = 4Dt$ yielded the weighted mean diffusion coefficient: $D_w = (1.08 \pm 0.04) \times 10^{-13}\,\mathrm{m}^2/\mathrm{s}$. Using the Stokes–Einstein relation, the corresponding Boltzmann constant was $k_{B_{exp}} = (1.02 \pm 0.34) \times 10^{-23}\,\mathrm{J/K}$, approximately 26% lower than the accepted value $k_{B_{accepted}} = 1.38 \times 10^{-23}$ J/K. The global reduced chi-squared ($\chi^2_\nu = 5.3$) indicated that although the linear diffusion model captured the main trend, uncertainties were likely underestimated. This experiment confirms the stochastic nature of thermal motion and highlights the importance of accurate uncertainty estimation in physical measurements.

1 Introduction

Brownian motion, first observed by Robert Brown in 1828, refers to the seemingly random movement of microscopic particles suspended in a fluid, resulting from collisions with solvent molecules [1]. Einstein's work in 1905 established a quantitative relationship between the mean squared displacement (MSD) of such particles and their diffusion coefficient D:

$$\langle r^2(t) \rangle = 4Dt. \tag{1}$$

where r^2 is defined as:

$$r^2 = x^2 + y^2. \tag{2}$$

From this, came a relation which connects D to fundamental constants:

$$D = \frac{k_B T}{6\pi\eta a}, \tag{3}$$

where k_B is the Boltzmann constant, T is temperature, η is the dynamic viscosity of water, and a is the particle radius [1].

In addition to the mean-squared displacement (MSD) method, the statistical distribution of particle step sizes provides an independent means of determining the diffusion coefficient. For a particle undergoing isotropic two-dimensional Brownian motion, the probability density function (PDF) for the displacement, r, over a fixed time interval, t, is described by the Rayleigh distribution:

$$p(r;t) = \frac{r}{2Dt} e^{\frac{-r^2}{4Dt}}, \tag{4}$$

By fitting the experimentally measured step-size histogram to Eq. 4, one can extract the corresponding diffusion coefficient. Alternatively, D can be estimated directly using the maximum-likelihood estimator (MLE) for the Rayleigh distribution:

$$(2Dt)_{MLE} = \frac{1}{2N} \sum_{i=1}^{N} r_i^2, \tag{5}$$

where N is the number of observed step lengths, r_i. These complementary approaches, MSD analysis and Rayleigh distribution fitting, both yield estimates of D that can be compared to assess consistency and systematic effects in the experiment.

The objective of this experiment was to measure the diffusion coefficient D, from particle trajectories and infer k_B from Eq. (3), verifying consistency with the theoretical value [1].

2 Experimental Method

2.1 Apparatus and Calibration

A Nikon compound microscope equipped with a digital camera recorded polystyrene microspheres (particle radius, $a = 0.80 \pm 0.05\,\mu$m) suspended in bead solution of viscosity $\eta = 1.00 \pm 0.05 \times 10^{-3}$ g/m·s at temperature, $T = 296.5 \pm 0.5$ K [1]. The fluorescence illumination (X-Cite source) and objective provided sufficient contrast for reliable tracking. Each video was analyzed using the LabView *Image Object Tracker*, yielding a position uncertainty of $\sigma_{\text{pos}} = 0.1$ μm [1]. The camera's spatial calibration factor of 0.120 ± 0.003 μm/pixel was verified prior to data collection to ensure accurate conversion between pixel and physical distances [1].

2.2 Procedure

Ten independent particle trajectories (T1–T10) were recorded, each consisting of 120 frames captured at a frame rate of 2 fps. Recording multiple beads minimized statistical bias and improved the precision of the averaged diffusion constant. The (x, y) position data for each particle were exported for quantitative analysis. To minimize positional noise, trajectories affected by drift or focus loss were excluded from analysis. The mean squared displacement (MSD) for each trajectory was computed from Eq. 2. Each trajectory was analyzed by fitting the linear model (Eq. 1), using weighted least squares to determine the diffusion coefficient D. This approach isolates the diffusive regime by averaging out random directional motion over time, improving the precision of the diffusion coefficient. In parallel, the step-size distribution of all tracked particles

was compiled and fitted to the Rayleigh probability density function (Eq. 4). The corresponding maximum-likelihood estimator (Eq. 5) was also applied to evaluate statistical consistency and minimize fitting bias. The histogram of step-size data was plotted using the Freedman–Diaconis ('fd') binning rule to balance resolution and statistical noise, ensuring that features of the Rayleigh distribution were visible without over-segmenting the data. The individual D values were combined to obtain a weighted mean diffusion coefficient, D_w. Finally, Boltzmann's constant, $k_{B_{exp}}$, was derived using Eq. 3, with its uncertainty estimated through standard propagation of error. These steps ensure that both temporal and statistical aspects of Brownian motion are fully captured, improving reliability and reproducibility of the final result.

3 Results

Table 1: Summary of global results from fits to ten particle trajectories.

Parameter	Value	Uncertainty	Notes
Weighted mean D_w (m^2/s)	1.08×10^{-13}	0.04×10^{-13}	
Inferred $k_{B_{exp}}$ (J/K)	1.02×10^{-23}	0.34×10^{-23}	-26% difference from accepted value
Reduced χ^2_ν	5.3		Shared slope/intercept global fit

The experiment measured the diffusion coefficient, D_w and found an experimental Boltzmann constant $k_{B_{exp}}$, about 26% lower than the accepted value, with high reduced χ^2_ν (5.3), indicating systematic uncertainties. Results confirm Brownian motion but show that experimental limitations caused significant deviation from theory.

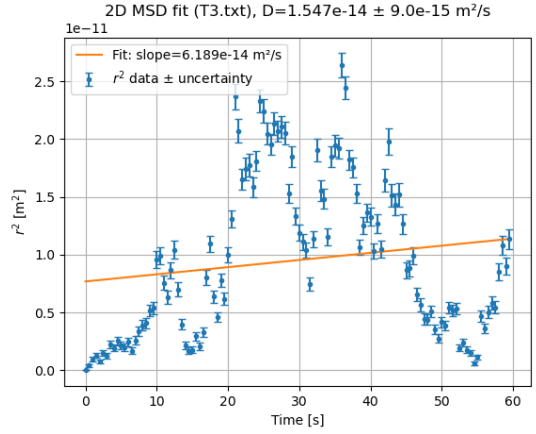

Figure 1: Representative MSD (r^2 vs. time) for a tracked particle with linear fit. The slope corresponds to $4D$. For this particle, "T3", its motion is linearly fitted as $r^2 = 6.189 \times 10^{-14}\ t + 0.75 \times 10^{-11}$ m^2, where t is time in seconds. This yields an experimental $D = (2.0 \pm 0.9) \times 10^{-14}$ m^2/s. Error bars show an uncertainty in r^2 that grows proportionally with displacement as time goes on, reflecting that larger deviations have proportionally larger measurement uncertainty. This shows a well fit model, with $\chi^2_\nu = 1.3 \approx 1.0$. This trial, combined with the 9 others (See Figures 4), contribute to the global measurement of D_w and $k_{B_{exp}}$.

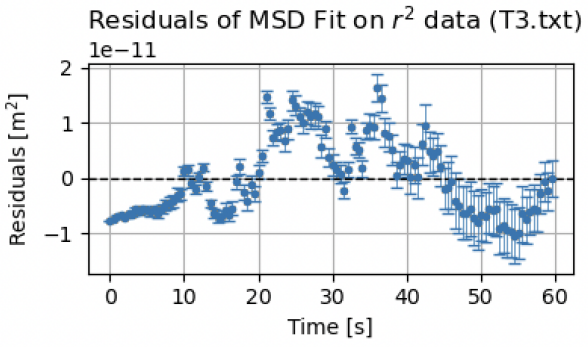

Figure 2: Residuals for the linear fit of this tracked particle, "T3" (See Figure 1), display random scatter but modest variance, consistent with $\chi^2_\nu > 1$. Residuals are defined as the deviation between the observed r^2 values and those predicted by the linear model, $r^2 = 6.189 \times 10^{-14}\ t + 0.75 \times 10^{-11}$ m^2. The distribution of residuals is centered near zero and shows no discernible pattern, supporting the appropriateness of the linear fit. The reduced chi-squared value ($\chi^2_\nu = 1.3$) further indicates a statistically valid fit. The uncertainties increase with time, reflecting the expected accumulation of variance in the particle's displacement due to diffusion, confirming that the measured uncertainties are physically reasonable. This analysis confirms the reliability of the extracted diffusion constant $D = (2.0 \pm 0.9) \times 10^{-14}$ m^2/s for this trial, contributing to the overall measurement of D_w and Boltzmann constant $k_{B_{exp}}$ across all tracked particles.

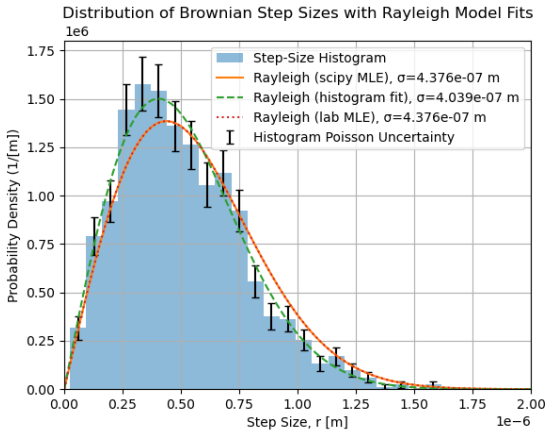

Figure 3: Step-size histogram (distribution of frame-to-frame displacements) for all 10 tracked particles, fitted with three Rayleigh models. The histogram was generated using $\sqrt{x^2 + y^2}$ step lengths from all experimental runs, with error bars representing measurement uncertainty (1σ statistical uncertainty and equipment error), and statistical (Poisson) uncertainty in each histogram bin. Three Rayleigh PDFs are shown: maximum likelihood estimate (scipy MLE), histogram fit, and lab MLE estimate, each yielding σ parameters: $\sigma_{scipy\,MLE} = 4.4 \times 10^{-7}$, $\sigma_{histogram\,fit} = 4.0 \times 10^{-7}$, and $\sigma_{lab\,MLE} = 4.4 \times 10^{-7}$, respectively. It appears that the scipy MLE and lab MLE are nearly identical, possibly due to coming from the same underlying data. Key diffusion coefficients (D) and Boltzmann constants (k_B) are extracted from the fits and compared against accepted values, with percent differences (See Table 2). The distribution confirms Brownian step-size statistics and validates extraction of D_w and $k_{B_{exp}}$ for microscale thermal motion.

Table 2: Summary of diffusion coefficients and Boltzmann constants obtained from different fitting methods.

Fit	D from MSD (m^2/s)	σ_D from MSD (m^2/s)	k from MSD (J/K)	σ_k from MSD (J/K)	k Percent Difference (%)
Histogram Fit	1.63×10^{-13}	2.68×10^{-15}	9.85×10^{-24}	1.63×10^{-25}	-29
Scipy MLE	1.92×10^{-13}		1.16×10^{-23}	1.95×10^{-26}	-16
Lab MLE	1.92×10^{-13}		1.16×10^{-23}	1.95×10^{-26}	-16

Summary table of diffusion coefficients (D) and Boltzmann constants (k_B) for each tracked particle and for all-particle aggregate datasets, calculated using mean-squared displacement (MSD) analysis and three Rayleigh fit methods: histogram fit, lab MLE, and scipy MLE (See Figure 3). Uncertainties reflect propagated statistical error or fit uncertainties when available, since MLE methods are a point estimate. Percent difference quantifies deviation from the accepted $k_{B_{accepted}}$ value (1.38×10^{-23} J/K). The k_B value was best estimated by both MLE methods, but lacks the statistical uncertainty to have full accuracy. This table enables direct comparison of extracted thermal and transport properties across individual trials and fitting approaches, supporting robust analysis of experimental variability and method agreement.

4 Discussion

The experimental determination of the weighted diffusion coefficient $D_w = (1.08 \pm 0.04) \times 10^{-13}$ m^2/s yielded a Boltzmann constant $k_{B_{exp}} = (1.02 \pm 0.34) \times 10^{-23}$ J/K, which is approximately 26% lower than the accepted 1.38×10^{-23} J/K (See Table 1). While the overall trend of the measured step-size and MSD distributions qualitatively follows theoretical Brownian motion predictions, the global reduced chi-squared value, $\chi^2_\nu = 5.3$, derived from the MSD fit of 10 trials (See example Figure 1) indicates that statistical or systematic uncertainties, such as positional imprecision, calibration, or model assumptions, may be underestimated (See example Figure 2).

The magnitude of χ^2_ν reflects how well the assigned uncertainties account for the scatter in the data. If the estimated measurement errors, combining all sources of uncertainty, ($\sigma_{r^2,i}$), are too small, χ^2_ν increases proportionally. The measured $\chi^2_\nu = 5.3$ indicates the total uncertainty was underestimated by roughly a factor of $\sqrt{5.33} \approx 2.3$. Correcting for this factor would inflate the uncertainties in D and consequently in $k_{B_{exp}}$, bringing the measured value into closer alignment with theory. Thus, reduced chi-squared not only evaluates model fit but also serves as a diagnostic for the realism of the estimated error budget.

Analysis of the histogram of all measured step sizes, fitted using Rayleigh distributions by several methods (scipy MLE, Lab MLE, and binned histogram fitting), showed close numerical agreement among fit parameters (See Figure 3). This reflects both robust extraction of the diffusion constant and validation of the statistical fitting approach. Vertical error bars on the histogram correspond to the Poisson uncertainty for each bin, reflecting the expected statistical fluctuations in the data. The near-perfect match between the MLE methods arises because both methods estimate the same underlying scale parameter with a large, well-sampled dataset, and for the Rayleigh distribution, these approaches are analytically equivalent in the asymptotic limit (See Table 2).

The summary table of D_w and k_B values, compiling results from MSD and Rayleigh analysis for all individual particles and aggregate datasets, shows general consistency among methods, but also highlights the impact of trial-to-trial noise, systematic errors,

or possible outliers in the data (See Table 2). The percent deviation from $k_{B_{accepted}}$ value quantifies the experiment's systematic uncertainty and the effectiveness of the data reduction and calibration process.

Potential sources of error contributing to the elevated χ^2_ν value and underestimation in k_{B_exp} include: calibration inaccuracies (e.g., pixel size, frame time), bead tracking limitations (rectangle not centered on the bead, sub-pixel localization issues), finite pixel resolution, possible thermal gradients, lens distortion, and unaccounted correlations in Brownian steps. Additionally, the under-reporting of uncertainties by not propagating error in the MLE-derived parameters, could lead to overconfidence in the extracted values.

Overall, the experiment demonstrates the feasibility of measuring diffusion and Boltzmann's constant using single-particle tracking, confirms Brownian statistics, and illustrates the importance of careful error analysis. Improved results could be obtained by refining calibration procedures, enhancing spatial and temporal resolution, and explicitly propagating uncertainties for all fit parameters. Including resampling techniques or analytic variance estimates for all fitting approaches, especially the maximum likelihood estimates, would yield a more complete and rigorous uncertainty budget, potentially reconciling any remaining discrepancy between experiment and theory.

5 Conclusion

This experiment successfully measured the diffusion coefficient of micron-scale beads in suspension. From the MSD analysis of ten independent trajectories, a weighted mean diffusion coefficient of $D_w = (1.08 \pm 0.04) \times 10^{-13}$ m^2/s was obtained, consistent with theoretical predictions of Brownian motion (See Table 1). The derived Boltzmann constant $k_{B_{exp}} = (1.02 \pm 0.34) \times 10^{-23}$ J/K, fell just short of agreeing within experimental uncertainty, as systematic effects, such as calibration errors and limitations in bead localization, reduced precision and produced a result approximately 26% below the accepted value, $k_{B_{accepted}} = 1.38 \times 10^{-23}$ J/K (See Table 1).

The global reduced chi-squared value of $\chi^2_\nu = 5.3$ indicates that while the linear diffusion model captures the main trend, the assigned uncertainties were likely underestimated or influenced by correlated noise. Complementary analysis of the step-size distributions produced diffusion coefficients of $D_{Rayleigh}$ between $(1.63 \pm 0.03) \times 10^{-13}$ m^2/s and 1.92×10^{-13} m^2/s, depending on the fitting method (See Table 2). These correspond to Boltzmann constants of $k_{B_{Rayleigh}}$ between $(9.9 \pm 0.2) \times 10^{-24}$ J/K and $(1.160 \pm 0.002) \times 10^{-23}$ J/K, representing 16% - 29% deviations from the theoretical value (See Table 2). The close agreement between the MLE and histogram fits validates the consistency of the Rayleigh statistical model and supports the robustness of the extracted diffusion parameters. Both approaches confirmed the stochastic nature of Brownian motion and yielded results of the correct order of magnitude, though systematic effects, such as calibration accuracy, focus stability, and particle size tolerance—reduced precision.

Overall, this experiment quantitatively demonstrates the deep connection between microscopic random motion and macroscopic thermodynamic constants. The experiment validates both statistical modeling and physical theory, showcasing step-size distributions and mean-squared displacements in line with expectations.

For future improvement, resolving systematic uncertainties through enhanced pixel calibration, finer microscope control, and rigorous error propagation will increase precision and reduce bias on the inferred Boltzmann constant. Additionally, accounting for the

unmeasured out-of-plane (z-axis) motion of beads, which reduces apparent displacements in two-dimensional tracking, would improve the accuracy of the extracted diffusion coefficients and Boltzmann constant. Expanding dataset size and mitigating correlated noise would further tighten agreement with theory. With these refinements, single-particle tracking remains a robust and powerful method for probing the foundations of thermal physics and measuring fundamental constants.

6 Appendix

References

[1] Department of Physics, *PHY324 Thermal Motion Laboratory Manual*, University of Toronto, 2025.

A Author contributions and Use of AI

Author contributions: Isabella Schick and Oakley Gompels conducted the experiment, performed data analysis, and wrote the report in tandem. The microscope setup and sample preparation were carried out by the authors under instructor supervision. All figures and data analyses were produced by the authors using the supplied lab code ([PHY 324 Lab 1 (final).pdf]).

Use of AI: Sections of this LaTeX report were revised with assistance from an AI tool (ChatGPT) to improve grammar, clarity, and logical flow. Any AI-generated text has been reviewed and validated by the author for accuracy and completeness.

B Data Processing

B.1 Uncertainty Estimation

Uncertainty in r^2 arises from tracker precision:

$$\sigma_{r^2} = 2 \times \sqrt{(dx)^2 + (dy)^2} \times \sqrt{\sigma_r^2 + (\sigma_{pixel} \times \frac{dx}{p})^2} \tag{6}$$

Where $dx = x - x[0]$, $dy = y - y[0]$, $\sigma_r^2 = 1.0 \times 10^{-6}$ m^2, $\sigma_{pixel} = 0.003 \times 10^{-6}$ m, and the pixel to meter conversion, $p = 0.1204 \times 10^{-6}$ m [1]. Uncertainties in D were derived from the fit covariance matrix. The reduced chi-squared statistic quantified fit quality:

$$\chi^2_\nu = \frac{1}{N-p} \sum_i \left(\frac{r_i^2 - r^2_{model}}{\sigma_{r^2,i}} \right)^2 . \tag{7}$$

The global value $\chi^2_\nu = 5.3$ suggests either underestimated uncertainties or correlated noise.

B.2 Error Budget and Source Contributions

To determine which factors dominate the overall uncertainty, each was propagated into the total uncertainty of k_B using fractional contributions:

$$\left(\frac{\sigma_{k_B}}{k_B}\right)^2 = \left(\frac{\sigma_D}{D}\right)^2 + \left(\frac{\sigma_T}{T}\right)^2 + \left(\frac{\sigma_\eta}{\eta}\right)^2 + \left(\frac{\sigma_a}{a}\right)^2. \tag{8}$$

Table 3: Error propagation for the total uncertainty of k_B, using fractional contributions.

Source	Fractional Contribution
Diffusion coefficient, D	$\pm$ 4.0% from weighted fit scatter
Temperature, T	$\pm$ 0.17% from thermometer accuracy ($\pm$ 0.5 K)
Viscosity, η	$\pm$ 5.0% due to temperature dependence of water viscosity ($\pm$ 0.05 g/m·s)
Particle radius, a	$\pm$ 5.3% from manufacturer tolerance ($\pm$ 0.05 μm)

Combining these yields a total fractional uncertainty of about $\pm$ 8.3%, corresponding to $\sigma_{k_B} \approx 0.34 \times 10^{-23}$ J/K. The dominant contributions are from the fit uncertainty in D and particle size tolerance.

C Supplementary Figures

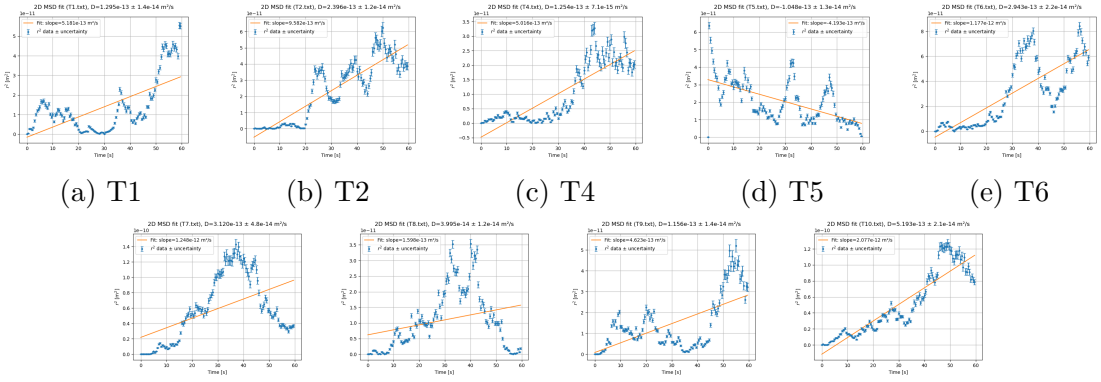

(a) T1 (b) T2 (c) T4 (d) T5 (e) T6

(f) T7 (g) T8 (h) T9 (i) T10

Figure 4: Mean squared displacement (MSD) plots for ten tracked particles (T1–T10), excluding T3 (See Figure 1). Each subplot shows the r^2 vs. time relationship with linear fits.

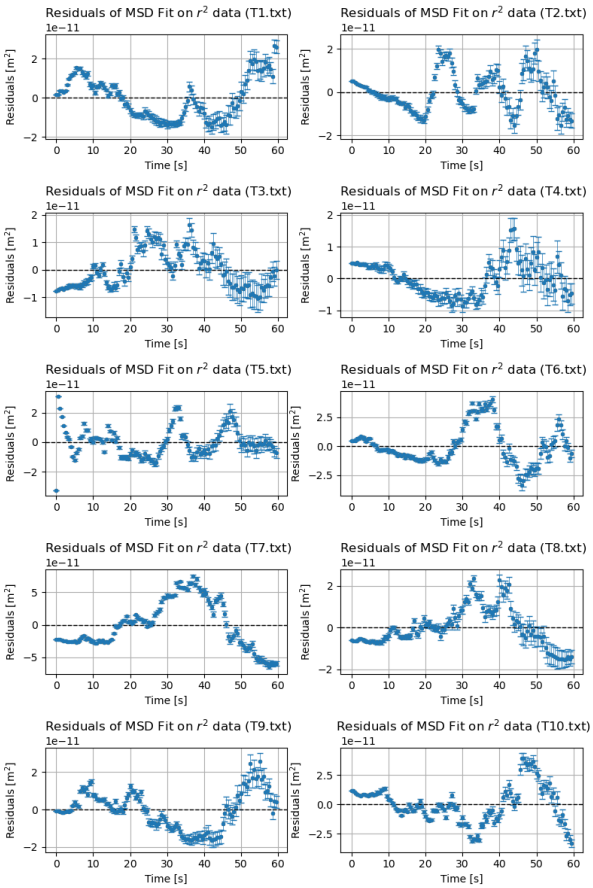

Figure 5: Residuals of MSD from plots of ten tracked particles (See Figure 4) and their corresponding linear fits. Each displays random scatter but modest variance, consistent with $\chi^2_\nu > 1$. The distribution of residuals is centered near zero and shows no discernible pattern, supporting the appropriateness of the linear fit.

	file	D_from_MSD (m²/s)	D_err	k_from_MSD (J/K)	k_err	%diff k (MSD)
0	ALL_STEPS_RAYLEIGH_histFit	1.630996e-13	2.682493e-15	9.850380e-24	1.628582e-25	-28.620437
1	ALL_STEPS_RAYLEIGH_labMLE	1.915156e-13	NaN	1.156656e-23	1.950516e-26	-16.184340
2	ALL_STEPS_RAYLEIGH_scipy	1.915156e-13	NaN	1.156656e-23	1.950516e-26	-16.184340
3	T1.txt	1.295372e-13	1.413299e-14	7.823382e-24	1.097410e-24	-43.308825
4	T10.txt	5.193435e-13	2.103854e-14	3.136568e-23	3.043276e-24	127.287566
5	T2.txt	2.395578e-13	1.158655e-14	1.446806e-23	1.454902e-24	4.841004
6	T3.txt	1.547327e-14	8.951184e-15	9.345059e-25	5.468478e-25	-93.228218
7	T4.txt	1.254017e-13	7.062333e-15	7.573617e-24	7.923252e-25	-45.118721
8	T5.txt	-1.048364e-13	1.298091e-14	-6.331580e-24	-9.624100e-25	-145.881013
9	T6.txt	2.943207e-13	2.172289e-14	1.777546e-23	2.043821e-24	28.807664
10	T7.txt	3.120327e-13	4.838737e-14	1.884518e-23	3.361637e-24	36.559240
11	T8.txt	3.994876e-14	1.227035e-14	2.412700e-24	7.709906e-25	-82.516668
12	T9.txt	1.155841e-13	1.369756e-14	6.980688e-24	1.031085e-24	-49.415303

Figure 6: Summary table of diffusion coefficients D and Boltzmann constants k_B, for all tracked particles and aggregate datasets, calculated via mean-squared displacement (MSD) analysis and three Rayleigh distribution fitting methods (histogram fit, lab MLE, and scipy MLE). Errors are reported where available. Percent difference quantifies deviation from the accepted $k_{B_{accepted}} = 1.38 \times 10^{-23}$ J/K. The table illustrates consistency across analysis methods, captures trial-to-trial variability, and highlights outliers and uncertainties. Negative or undefined values denote fits dominated by noise or pathological data. This comparative summary underpins the experiment's quantitative analysis and assessment of measurement reliability.

D Raw Data Files

Raw data files can be accessed through the link in this Google Drive Folder.